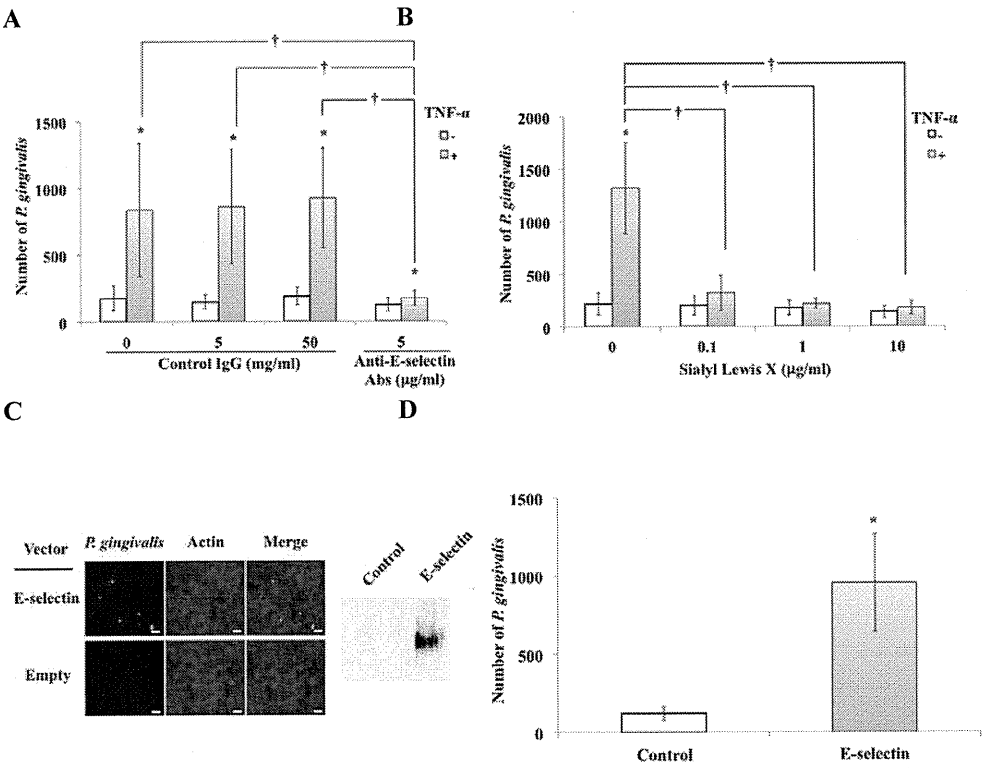

Komatsu *et al.* Fig. 2.

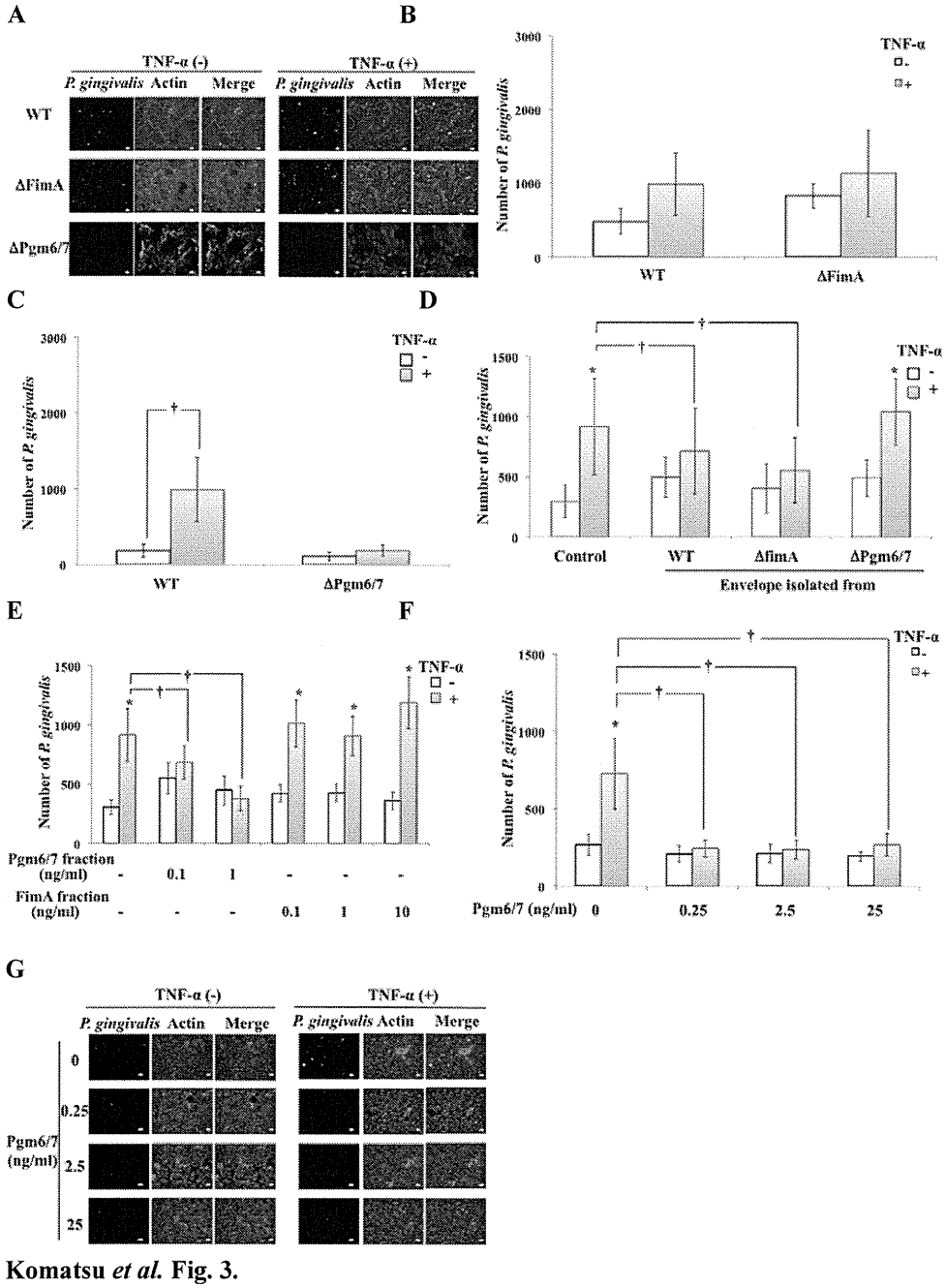

Komatsu *et al.* Fig. 3.

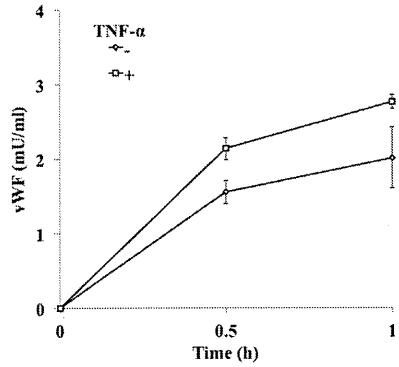

Komatsu *et al.* Fig. 4

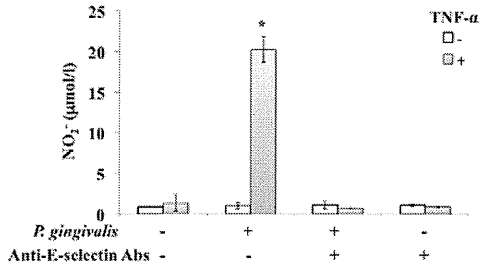

Komatsu *et al.* Fig. 5.

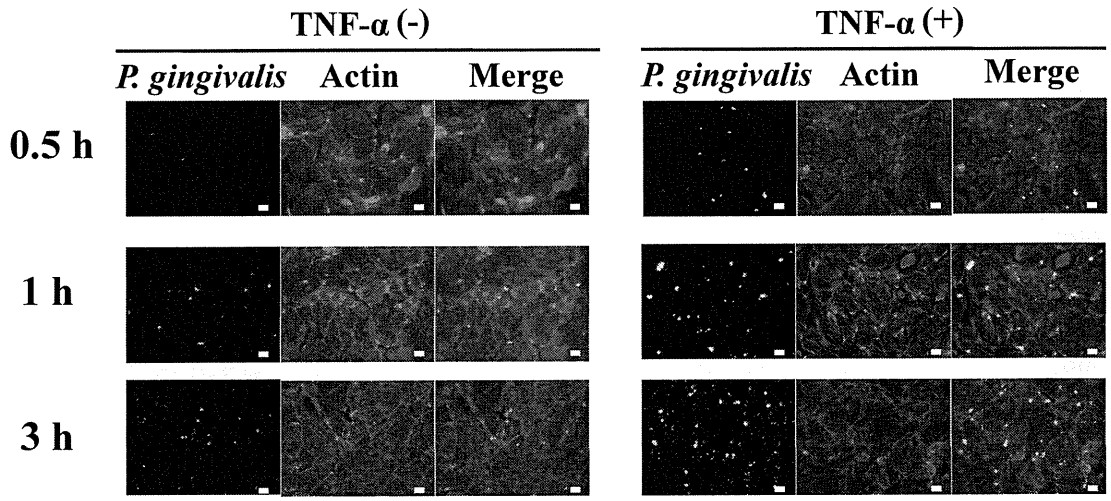

Figure 1. Adherence of *P. gingivalis* to HUVECs was enhanced by stimulation with TNF-α. (A) HUVECs were incubated with TNF-α (10 ng/ml) for 0.5-3 h. Then *P. gingivalis* ATCC 33277 cells (10^8 cells/ml/well) were added to the culture medium for 0.5-3 h. Cells were then washed and attachment of *P.gingivalis* to the cells was observed by fluorescent microscopy. *P. gingivalis* was stained with FITC (green), and actin of endothelial cells was visualized with TRITC (red). Scale bar is 10 μm.

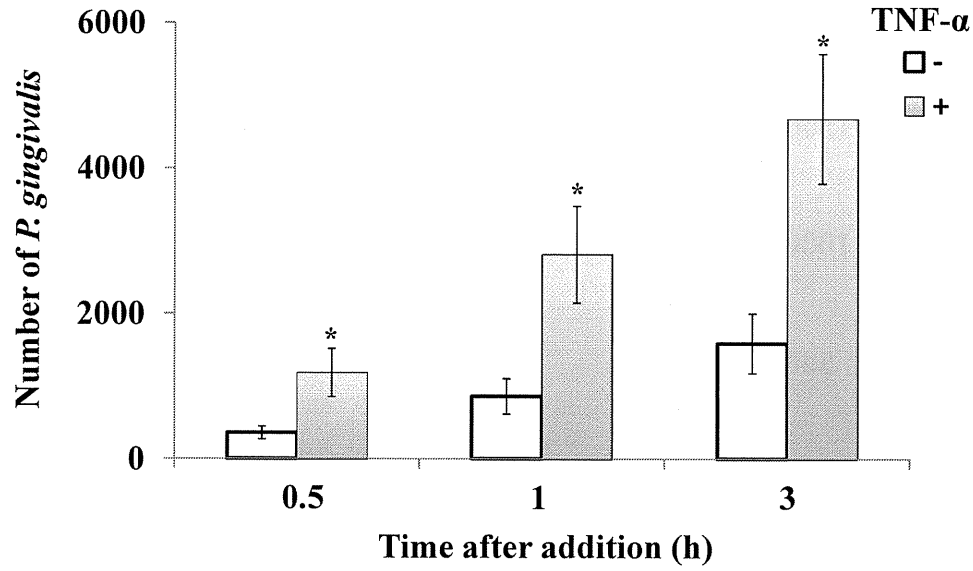

Figure 1. Adherence of *P. gingivalis* to HUVECs was enhanced by stimulation with TNF-α. (B) HUVECs were incubated with TNF-α (10 ng/ml) for 0.5-3 h. Then *P. gingivalis* ATCC 33277 cells (10^8 cells/ml/well) were added to the culture medium for 0.5-3 h. Cells were then washed and attachment of *P. gingivalis* to the cells was observed by fluorescent microscopy. The attachment levels were expressed as number of *P. gingivalis* cells per 60430 mm^2 (n = 3, means ± SD; $*P < 0.01$ vs no TNF-α).

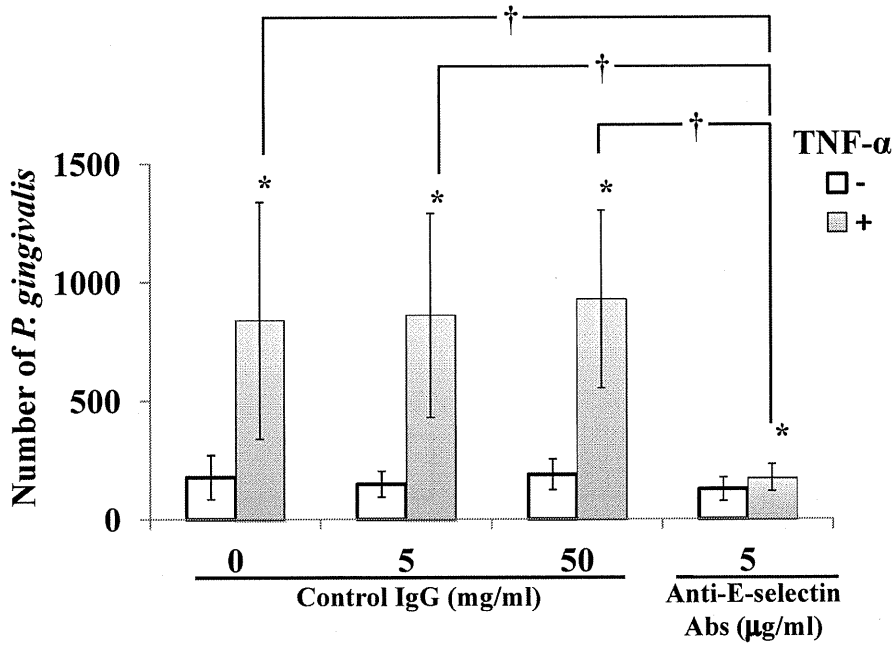

Figure 2. Adherence of *P. gingivalis* to TNF-α-activated endothelial cells was mediated by E-selectin. (A) Inhibitory effect of anti-E-selectin antibodies. HUVECs were incubated with TNF-α (10 ng/ml) for 3 h. Cells were then washed and incubated with *P. gingivalis* ATCC 33277 (10^8 cells/ml/well) for 30 min in the presence of an antibody for E-selectin or control IgG. Other procedures are described in the legend to Fig. 1B. (n = 3, means ± SD; **P* < 0.01 vs no TNF-α, †*P* < 0.01 vs. no Anti-E-selectin Abs).

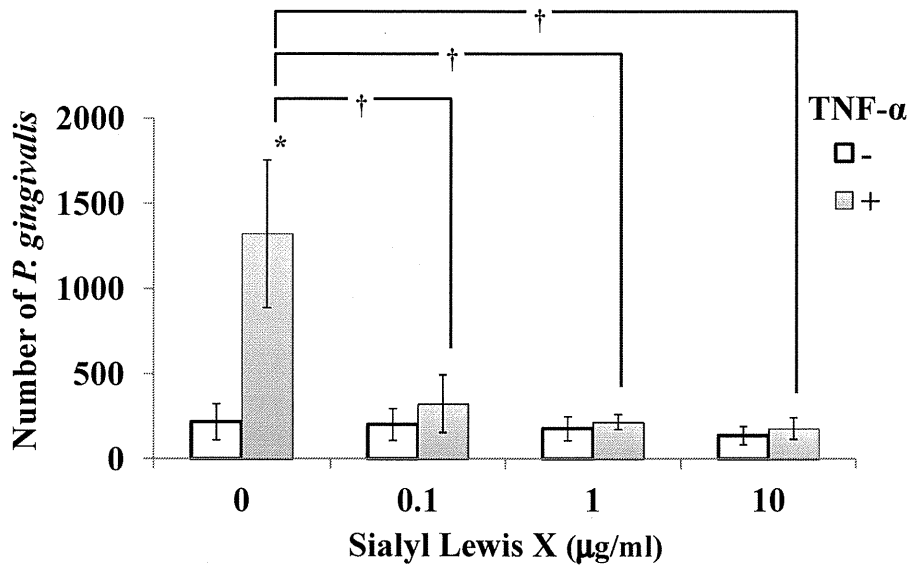

Figure 2. Adherence of *P. gingivalis* to TNF-α-activated endothelial cells was mediated by E-selectin. (B) Inhibitory effect of sialyl Lewis X. HUVECs were incubated with TNF-α (10 ng/ml) for 30 min. Cells were then washed and incubated with *P. gingivalis* ATCC 33277 (10^8 cells/ml/well) for 3 h in the presence of purified sialyl Lewis X (0-10 ng/ml). Other procedures are described in the legend to Fig. 1B. (n = 3, means ± SD; **P* < 0.01 vs. no TNF-α, †*P* < 0.01 vs. no sialyl Lewis X).

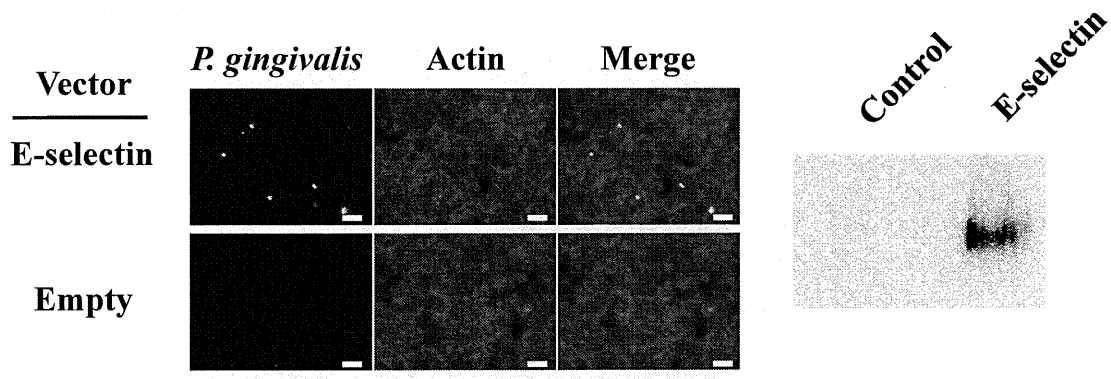

Adherence of *P. gingivalis* to TNF-α-activated endothelial cells was mediated by E-selectin. (C) Adherence of *P. gingivalis* was augmented in HEK293 cells transfected with an expression with vector for E-selectin. *P. gingivalis* ATCC 33277 (10^8 cells/ml/well) was incubated with HEK 293 cells transfected with a human E-selectin-inserted vector for 3 h. Other procedures are described in the legend to Fig. 1A. Scale bar is 10 μm.

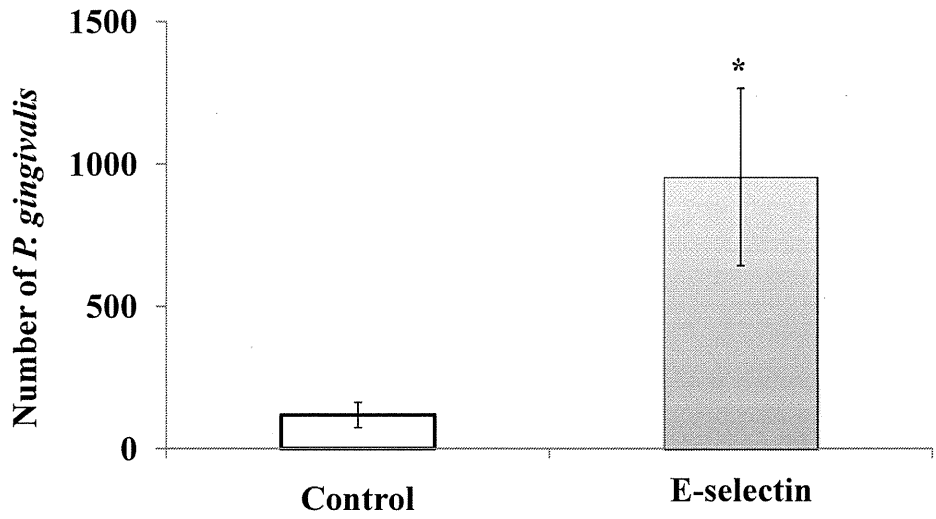

Adherence of *P. gingivalis* to TNF-α-activated endothelial cells was mediated by E-selectin. (D) Adherence of *P. gingivalis* was augmented in 293 cells transfected with an expression vector for E-selectin. *P. gingivalis* ATCC 33277 (10^8 cells/ml/well) was incubated with 293 cells transfected with a human E-selectin-inserted vector for 30 min. Other procedures are described in the legend to Fig. 1B. (n = 3, means ± SD; $*P < 0.01$ vs. control).

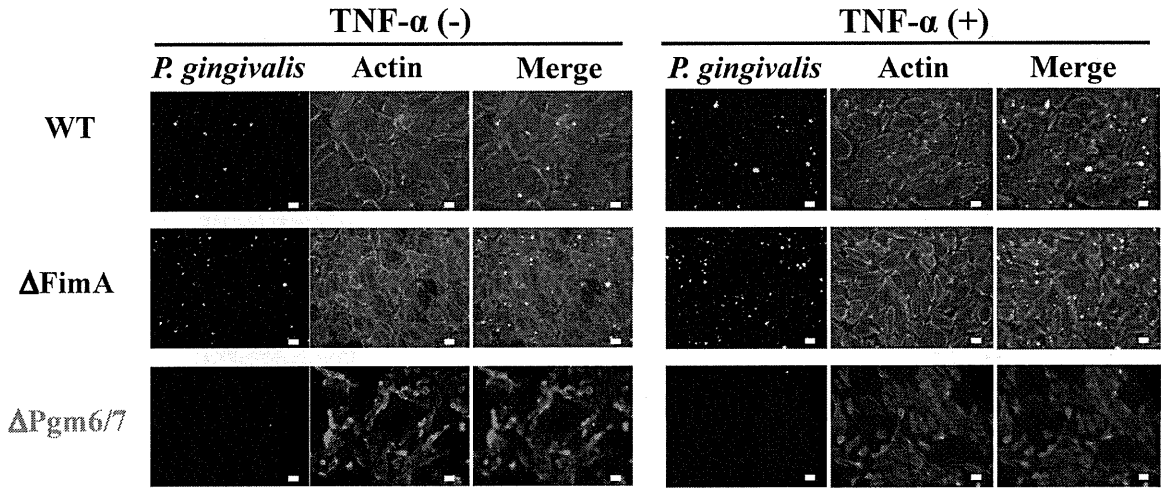

Figure 3. Pgm6/7 in *P. gingivalis* mediated the interaction with activated endothelial cells. (A) *P. gingivalis* ATCC 33277 (wild type), FimA-deficient mutant (ΔFimA), and Pgm6/7-deficient mutant (ΔPgm6/7) (10^8 cells/ml/well) were incubated with TNF-α-pretreated HUVECs for 3 h, respectively. Other procedures are described in the legend to Fig. 1A. Scale bar is 10 μm.

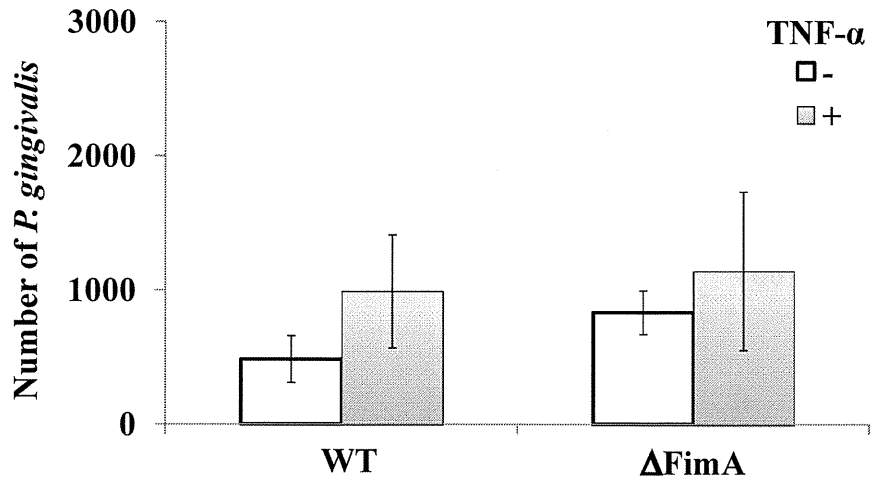

Figure 3. Pgm6/7 in *P. gingivalis* mediated the interaction with activated endothelial cells. (B) *P. gingivalis* ATCC 33277 (wild type) and FimA-deficient mutant (ΔFimA) (10^8 cells/ml/well) were incubated with TNF-α-pretreated HUVECs for 30 min, respectively. Other procedures are described in the legend to Fig. 1A. Scale bar is 10 μm.

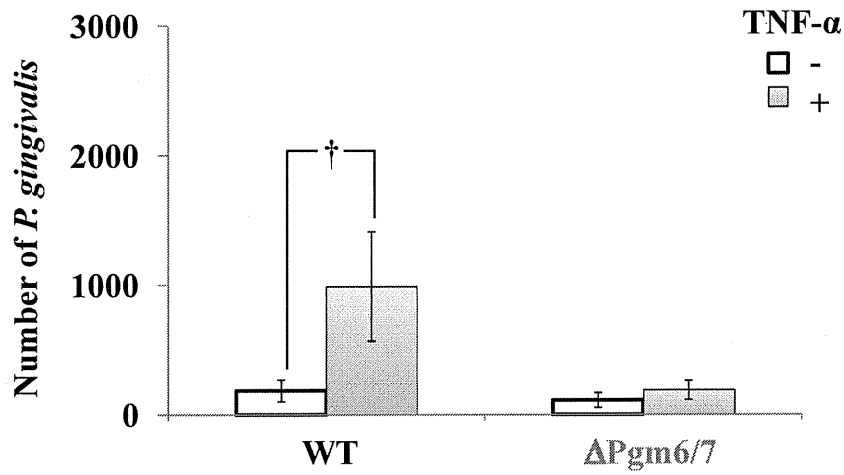

Figure 3. Pgm6/7 in *P. gingivalis* mediated the interaction with activated endothelial cells. (C) *P. gingivalis* ATCC 33277 (wild type) and Pgm6/7-deficient mutant (ΔPgm6/7) (10^8 cells/ml/well) were incubated with TNF-α-pretreated HUVECs for 30 min, respectively. Other procedures are described in the legend to Fig. 1B. (n = 3, means ± SD; $*P < 0.01$ vs. no TNF-α).

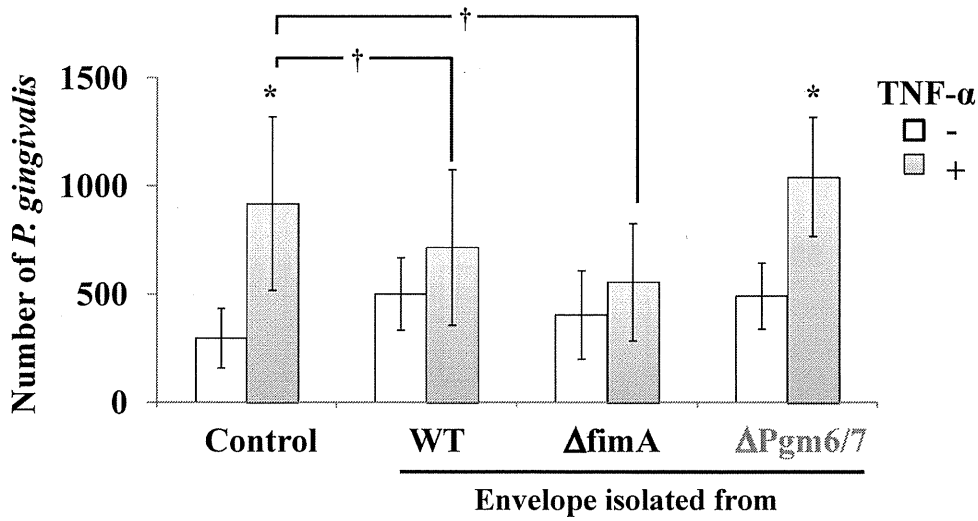

Figure 3. Pgm6/7 in *P. gingivalis* mediated the interaction with activated endothelial cells. (D) Inhibitory effects of *P. gingivalis* envelopes on TNF-α-induced adhesion of *P. gingivalis* to HUVECs. HUVECs were incubated with TNF-α (10 ng/ml) for 30 min. Cells were then washed and incubated with *P. gingivalis* ATCC 33277 (10^8 cells/ml/well) for 30 min in the presence or absence of envelopes isolated from wild-type or mutant *P. gingivalis*. Other procedures are described in the legend to Fig. 1B. (n = 3, means ± SD; **P* < 0.01 vs. no TNF-α, †*P* < 0.01 vs. control).

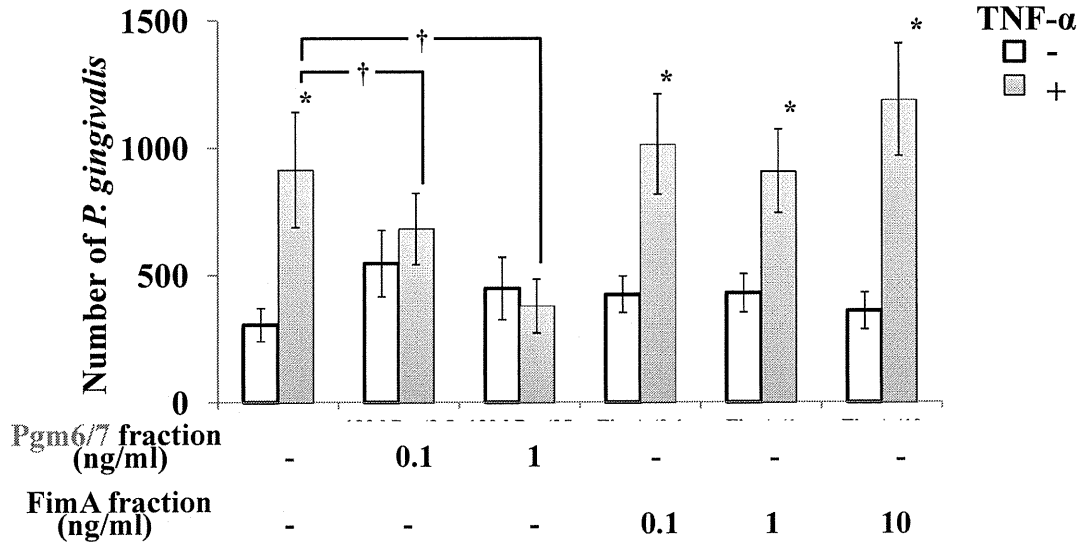

Figure 3. Pgm6/7 in *P. gingivalis* mediated the interaction with activated endothelial cells. (E) Effects of extracted Pgm6/7 and FimA on TNF-α-induced adhesion of *P. gingivalis* to HUVECs. HUVECs were incubated with TNF-α (10 ng/ml) for 30 min. Cells were then washed and incubated with *P. gingivalis* ATCC 33277 (10^8 cells/ ml/well) for 30 min in the presence or absence of purified Pgm6/7 and FimA. Other procedures are described in the legend to Fig. 1B. (n = 3, means ± SD; *$P < 0.01$ vs. no TNF-α, †$P < 0.01$ vs. Pgm6/7 fraction).

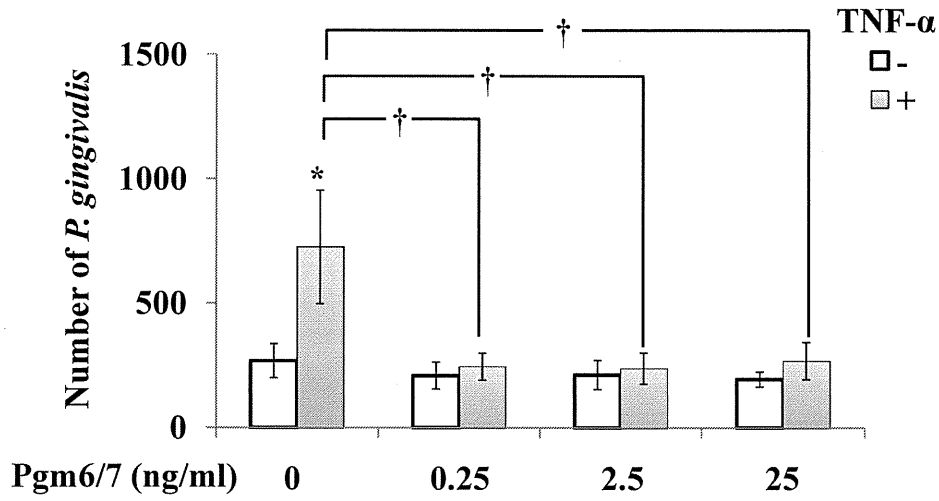

Figure 3. Pgm6/7 in *P. gingivalis* mediated the interaction with activated endothelial cells. (F) Inhibitory effect of *P. gingivalis* Pgm6/7 on TNF-α (10 ng/ml)-induced adhesion of *P. gingivalis* to HUVECs. HUVECs were incubated with TNF-α (10 ng/ml) for 30 min. Cells were then washed and incubated with *P. gingivalis* ATCC 33277 (10^8 cells/ ml/well) for 30 min in the presence or absence of purified Pgm6/7. Other procedures are described in the legend to Fig. 1B. (n = 3, means ± SD; **P* < 0.01 vs. no TNF-α, †*P* < 0.01 vs. Pgm6/7 0 ng/ml).

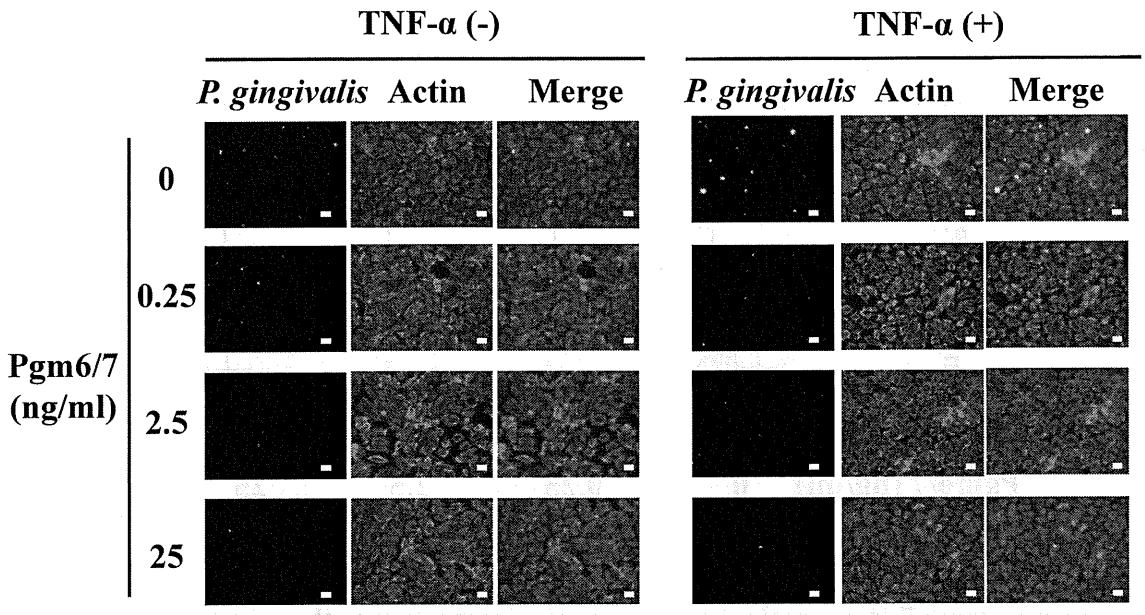

Figure 3. Pgm6/7 in *P. gingivalis* mediated the interaction with activated endothelial cells. (G) Inhibitory effect of *P. gingivalis* Pgm6/7 on TNF-α-induced adhesion of *P. gingivalis* to HUVECs. HUVECs were incubated with TNF-α (10 ng/ml) for 30 min. Cells were then washed and incubated with *P. gingivalis* ATCC 33277 (10^8 cells/ml/well) for 30 min in the presence or absence of purified Pgm6/7. Other procedures are described in the legend to Fig. 1A. Scale bar is 10 μm.

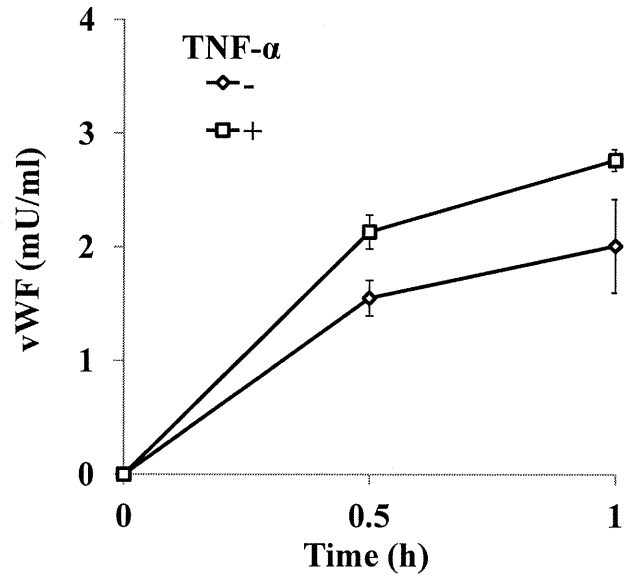

Figure 4. Endothelial vWF exocytosis to *P. gingivalis* were augmented by pretreatment with TNF-α. HUVECs were incubated with TNF-α (10 ng/ml) for 3 h. Cells were then washed and incubated with *P. gingivalis* ATCC 33277 (10^8 cells/ml/well) for 0-1 h. Then the release of vWF into media was measured by ELISA. (n = 3, means ± SD)

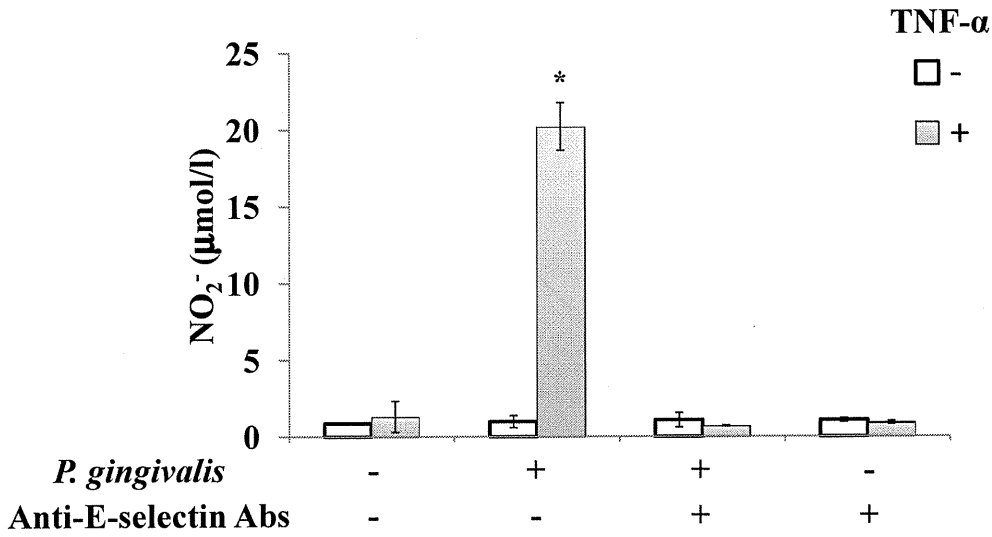

Figure 5. *P. gingivalis*-induced nitric oxide release from activated endothelial cells was mediated by E-selectin. HUVECs were incubated with TNF-α (10 ng/ml) for 3 h. Cells were then washed and incubated with *P. gingivalis* ATCC 33277 (10^8 cells/ml/well) for 30 min in the presence or absence of an antibody for E-selectin. Then the release of nitric oxide into media was measured by DAN assay (n = 3, means ± SD; **P* < 0.01 vs no TNF-α).

DNA Methylation Dynamics in Human Induced Pluripotent Stem Cells over Time

Koichiro Nishino, Masashi Toyoda, Mayu Yamazaki-Inoue, Yoshihiro Fukawatase, Emi Chikazawa, Hironari Sakaguchi, Hidenori Akutsu, Akihiro Umezawa*

Department of Reproductive Biology, National Institute for Child Health and Development, Tokyo, Japan

Abstract

Epigenetic reprogramming is a critical event in the generation of induced pluripotent stem cells (iPSCs). Here, we determined the DNA methylation profiles of 22 human iPSC lines derived from five different cell types (human endometrium, placental artery endothelium, amnion, fetal lung fibroblast, and menstrual blood cell) and five human embryonic stem cell (ESC) lines, and we followed the aberrant methylation sites in iPSCs for up to 42 weeks. The iPSCs exhibited distinct epigenetic differences from ESCs, which were caused by aberrant methylation at early passages. Multiple appearances and then disappearances of random aberrant methylation were detected throughout iPSC reprogramming. Continuous passaging of the iPSCs diminished the differences between iPSCs and ESCs, implying that iPSCs lose the characteristics inherited from the parent cells and adapt to very closely resemble ESCs over time. Human iPSCs were gradually reprogrammed through the "convergence" of aberrant hyper-methylation events that continuously appeared in a de novo manner. This iPS reprogramming consisted of stochastic de novo methylation and selection/fixation of methylation in an environment suitable for ESCs. Taken together, random methylation and convergence are driving forces for long-term reprogramming of iPSCs to ESCs.

Citation: Nishino K, Toyoda M, Yamazaki-Inoue M, Fukawatase Y, Chikazawa E, et al. (2011) DNA Methylation Dynamics in Human Induced Pluripotent Stem Cells over Time. PLoS Genet 7(5): e1002085. doi:10.1371/journal.pgen.1002085

Editor: John M. Greally, Albert Einstein College of Medicine, United States of America

Received December 2, 2010; **Accepted** April 1, 2011; **Published** May 26, 2011

Funding: This research was supported by grants from the Ministry of Education, Culture, Sports, Science, and Technology (MEXT) of Japan; by Ministry of Health, Labour, and Welfare Sciences (MHLW) research grants; by a Research Grant on Health Science focusing on Drug Innovation from the Japan Health Science Foundation; by the program for the promotion of Fundamental Studies in Health Science of the Pharmaceuticals and Medical Devices Agency; by a Grant for Child Health and Development from the MHLW; by the Intramural Research Grant (22-5) for Neurological and Psychiatric Disorders of NCNP; by the Research Grant (22-2-4) for cardiovascular disease of NCVC given to AU; by a grant from New Energy and Industrial Technology Development Organization (NEDO) in Japan given to HA; and by Grant-in-Aid for Young Scientist(B)(WAKATE- B 21790372) given to KN. The funders had no role in study design, data collection and analysis, decision to publish, or preparation of the manuscript.

Competing Interests: The authors have declared that no competing interests exist.

* E-mail: umezawa@1985.jukuin.keio.ac.jp

Introduction

DNA methylation is an important epigenetic modification and is a key component in normal differentiation, development and disease [1–3]. Expression of tissue-specific genes, such as *Oct-4* [4], *Nanog* [5], *Sry* (sex determining region on Y chromosome) [6] and *MyoD* [7], are induced by spatio-temporal demethylation during development. DNA methylation therefore specifically varies depending on tissue types and cell linage [2], indicating that information regarding cell type-specific DNA methylation profiles can enable the identification and validation of cell types. Transformation of iPSCs from somatic cells requires a process of epigenetic reprogramming promoted by transient ectopic expression of defined transcription factors expressed in ESCs [8–11]. Human iPSCs are considered to be powerful resources in regenerative medicine because of their potential of pluripotency and avoidance of rejection of their derivatives by the immune system, and for ethical issues as well [12]. Although iPSCs show pluripotency, they have different propensities for differentiation in mouse models [13]. Human iPSCs also exhibit donor cell-specific gene expression [14,15]. Moreover, iPSCs possess inherited DNA methylation states as epigenetic memories from parent cells [15–17], suggesting that these memories influence different propensities of the iPSCs. On the other hand, continuous passaging of mouse iPSCs reduces differences from each other in gene expression profiles [15]. Epigenome-wide analysis started to be used in this field [18,19], and differentially methylated regions have been identified among human iPSCs, their parent cells and ESCs [17,20]. Aberrant epigenetic reprogramming has recently been reported in human iPSCs [21,22]. However, these analyses were limited to the use of a small number of cells as a source for generation of iPS cells. Moreover, human iPSCs have only been analyzed at a single point of passage. Therefore, it has not been clarified whether human iPSCs generated from various types of cells are dissimilar from each other at different points during passage; how continuous passaging of human iPSCs influences the differences between iPSCs and ESCs; and how aberrant methylation in human iPSCs during passaging. To address these issues, we compared the epigenetic and transcriptional states of human iPSCs derived from five cell types of different origins during passage, and found random aberrant hyper-methylation at different points of adaptation into ESCs.

Results

Establishment of human iPSCs

Human iPSCs derived from fetal lung fibroblasts (MRC5), amnion (AM), endometrium (UtE), placental artery endothelium (PAE) and menstrual blood cells (Edom) were independently established in our laboratory by retroviral infection of 4 genes